Journal Name

ARTICLE

Surface Functionalized Silica Nanoparticles for the Off-On Fluorogenic Detection of an Improvised Explosive, TATP, in a Vapour Flow †

Received 00th January 20xx,
Accepted 00th January 20xx

DOI: 10.1039/x0xx00000x

www.rsc.org/

José García-Calvo,[a] Patricia Calvo-Gredilla,[a] Marcos Ibáñez-Llorente,[a] Daisy C. Romero,[a] José V. Cuevas,[a] Gabriel García-Herbosa,[a] Manuel Avella,[b] Tomás Torroba[a,*]

We report the development of new fluorogenic silica nanomaterials that were able to generate fluorescence in the presence of vapours of triacetone triperoxide, TATP, an improvised explosive used in terrorist attacks. The materials worked in a vapour flow of TATP, giving a permanent and strongly fluorescent response.

Introduction

Triacetone triperoxide (TATP) is a powerful explosive without military use due to high sensitivity to mechanical shock and difficulty to safe handling.[1] TATP is easily prepared from acetone and hydrogen peroxide under acidic catalysis.[2] It constitutes an improvised explosive almost undetectable by dogs or sniffer devices, usually trained for nitrogen-containing explosives.[3] TATP has been frequently used in suicide terrorist attacks, constituting an important threat in mass events and public transport.[4] The lack of nitro groups or aromatic moieties makes the detection of this improvised explosive a difficult task.[5] TATP is usually detected by mass spectrometry,[6] ion mobility spectrometry,[7] or multiphoton spectroscopy,[8] but the signature of TATP is not clearly visible except by bulky MS spectrometers.[9] As a consequence, portable and selective systems still need to be developed. Good alternatives are chemically modified nanosensor arrays,[10] or optical portable methods based on colorimetric sensor arrays that detect hydrogen peroxide (H_2O_2) from TATP decomposition.[11] Indirect detection of H_2O_2 from TATP, linked to oxidative processes,[12] was successfully used for colorimetric[13] or fluorimetric[12b,14] sensing. TATP direct detection has been achieved by fluorescence quenching[15] or quartz crystal microbalances.[16] Turn-on fluorogenic chemosensing systems are a good alternative for many analytes,[17] therefore fluorogenic probes that are specific for TATP are valuable methods for the detection of peroxide explosives. Perylenemonoimides (PMIs)[18] as well as perylenediimides (PDIs)[19] are strongly fluorescent compounds, stable under light and air, so they are good candidates for the search of new fluorogenic reporters. PMIs/PDIs bear an electron poor π-conjugated aromatic core, suitable for multiple chemical modifications and optical sensing,[20] that could be appropriate for the selective detection of pristine TATP in the vapour phase, a major as yet unresolved issue.[21] Our approach consisted of modifying the fluorescent PMI and PDI core with donor groups by established Suzuki coupling[22] to obtain compounds suitable for anchoring to silica surfaces, on the way to solid fluorogenic sensors for the sensitive and selective detection of TATP in the vapour phase. From the initial tests, we discovered that a modification of the PMI and PDI core with a substituted pyridyl group was able to modulate the electron donor-acceptor effect on the fluorescent core, giving products with an outstanding performance in terms of selectivity and sensitivity to TATP, that were suitable for their covalent anchoring to silica matrixes. Therefore, we want to report now the preparation of new surface modified fluorogenic silica materials for the selective detection of TATP in a vapour flow.

Results and discussion

We prepared PMIs/PDIs having one *p*-aminopyridyl group, to study their suitable characteristics and sensitivity to oxidants and their covalent anchoring to silica materials having a protective *N*-Boc group **JG125**/**PC63**, the unprotected compounds **JG125d**/**PC63d**, obtained by acidic deprotection, and the functionalized triethoxysilyl derivatives **JG131**/**JG135** (for details about the preparation, see the Supporting Information) (Figure 1). Compounds **JG125**/**JG125d** and **PC63**/**PC63d** were purple coloured compounds moderately fluorescent in some common organic solvents. Remarkably, **JG125** and **PC63** were extremely sensitive to TATP by turn-on fluorescent changes. For **JG125** (2.5·μM, λ_{exc} = 500 nm, λ_{em} = 556 nm) we got an increase in the quantum yield from Φ_{JG125} ($CHCl_3$) = 0.23 ± 0.01 to $\Phi_{JG125+TATP}$ ($CHCl_3$) = 0.65 ± 0.01 in the

[a] Department of Chemistry, Faculty of Science, University of Burgos, 09001 Burgos, Spain.
[b] Advanced Microscopy Unit, Scientific Park Foundation, I+D Building, Miguel Delibes Campus, University of Valladolid, 47011 Valladolid, Spain.

† Electronic Supplementary Information (ESI) available: Experimental details, characterization data, and additional experiments. See DOI: 10.1039/x0xx00000x

presence of TATP, with an overall increase of $\Phi_{JG125+TATP}/\Phi_{JG125}$ = 2.8; we got a limit of detection of 620 µM [0.11 mg/mL] for TATP in a $CHCl_3$:MeOH 9:1 solution. For **PC63** (2.5·µM, λ_{exc} = 484 nm, λ_{em} = 536 nm) we also got an increase in the quantum yield from Φ_{PC63} ($CHCl_3$) = 0.27 ± 0.01 to $\Phi_{PC63+TATP}$ ($CHCl_3$) = 0.36 ± 0.01, and a lower overall increase of $\Phi_{PC63+TATP}/\Phi_{PC63}$ = 1.3; the limit of detection for TATP was 4.83 mM [0.84 mg/mL] in a $CHCl_3$:MeOH 9:1 solution. Therefore, both compounds were suitable for the preparation of TATP detection materials. Appropriate products **JG131/JG135** for silica anchoring were obtained from **JG125d/PC63d** by reaction with 3-isocyanatopropyl triethoxy silane (Figure 1).

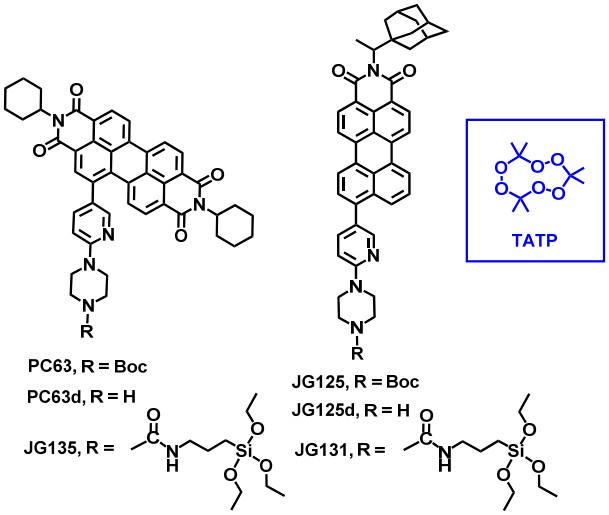

Figure 1 PMI/PDI derivatives used for TATP detection.

For the anchoring of silylated peryleneimides we used commercial silica nanoparticles, 10-20 nm, and TLC plates (silicagel 60, aluminium sheets 5x10 cm). Functionalized silica nanoparticles were prepared from 500 mg of pristine silica nanoparticles and 4 mg of the triethoxysilyl perylene derivatives **JG131** and **JG135**. The mixtures were refluxed at 112°C in a mixture of toluene:water (500:10 µL) for 24 hours, finally, the nanoparticles were washed with toluene, DCM and Et_2O. The materials obtained were labelled **nJG131** and **nJG135** (Figure 2). By the same way, the silane derivatives were bonded to silica TLC plates, 0.5 mg of **JG131** or **JG135** for every 5x10 cm plate. Instead of reflux, the plates were heated at 60°C for 48 hours, until the solutions had neither colour nor fluorescence. Then, the TLC plates were cleaned by the same procedure used in previous case. The materials obtained were labelled **pJG131** and **pJG135** (Figure 3). With the purpose of comparison to purely adsorbed materials, **JG125** and **PC63** were mixed with TLC plates under similar conditions to get the products adsorbed on silica, labelled **aJG125** and **aPC63**. We then checked colour and fluorescence qualitative and quantitative changes of all solid materials in the presence of TATP in the gas phase.

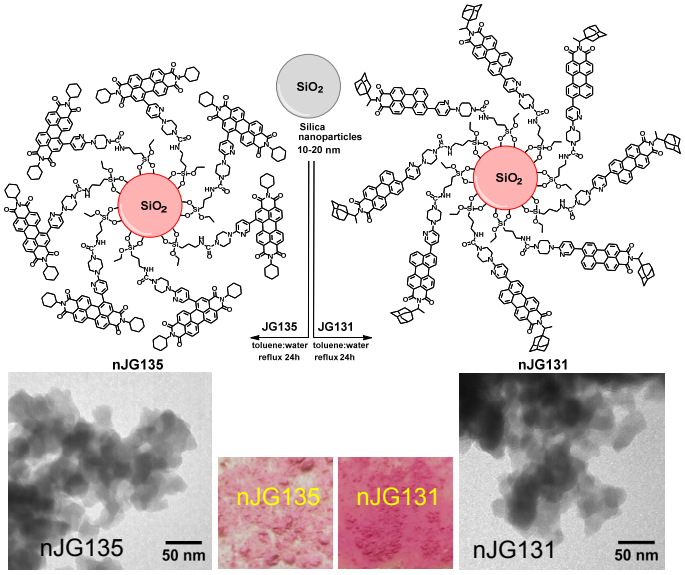

Figure 2 Preparation of **nJG131** and **nJG135**, TEM and day-light images of **nJG131** and **nJG135**.

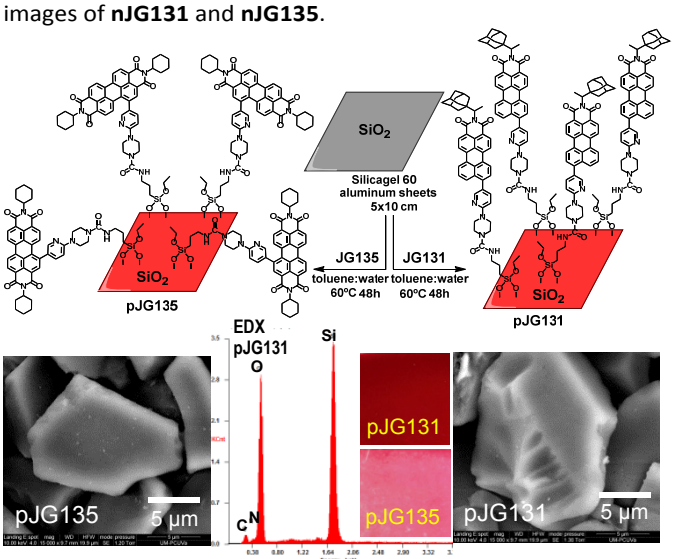

Figure 3 Preparation of **pJG131** and **pJG135**. SEM and day-light images of **pJG131** and **pJG135**. Inset: EDX profile of **pJG131**.

We started by checking colour and fluorescence qualitative and quantitative changes of solid materials **nJG131** and **nJG135** in the presence of TATP in a vapour flow. Silica nanoparticles were fixed to borosilicate glass coverslips 18 mm × 18 mm by spray adhesive and placed in a glassware system schematized in Figure 4. Every experiment employed 2 mg TATP and a dry nitrogen gas flow adjusted to 100 cm^3/min in a round bottom flask, gently warmed below 50°C with an external air flow heating (a laboratory hot air gun) for 10 min. The gas flow having an average concentration of 0.2 mg/L of evaporated TATP was conducted through a glassware tube to another similar flask at room temperature containing the solid sensor. Then the gas flow was finally vented through a glassware tube to exhaust (Figure 4) and the sensor material checked for changes in colour and fluorescence. We also checked the action of hydrochloric acid vapour (1 mL, 35% aqueous HCl, 30 seconds), acetic acid vapour (glacial AcOH vapour, 1 mL, 30 seconds), triethylamine vapour (neat NEt_3

vapour, 1 mL, 30 seconds) and hydrogen peroxide vapour (5 mL, 30% aqueous H_2O_2 for 10 minutes) under related conditions in order to assess the selectivity of the detection system (Figure 5).

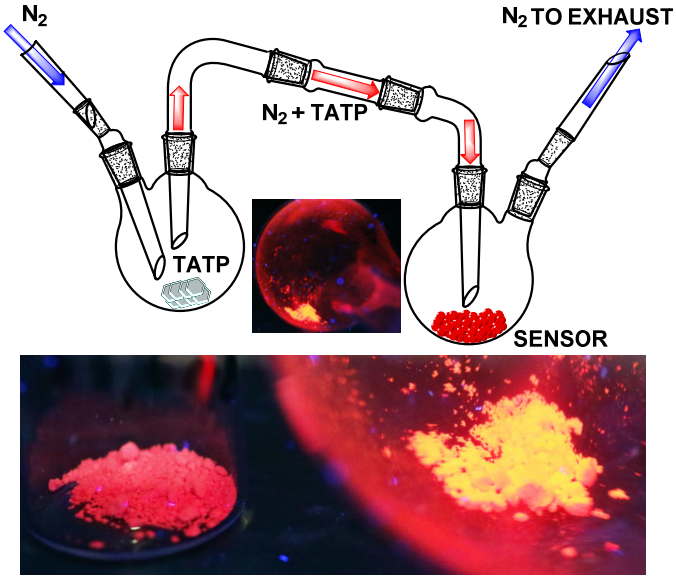

Figure 4 Upper: Glassware system design for the detection of TATP in the gas phase with **nJG131/pJG131** and **nJG135/pJG135**. Inset: Image of the right flask under UV light, 366 nm, after TATP experiment. Lower: **JG131** nanoparticles (left) as prepared and (right) after treatment with TATP vapour, both under UV light, 366 nm.

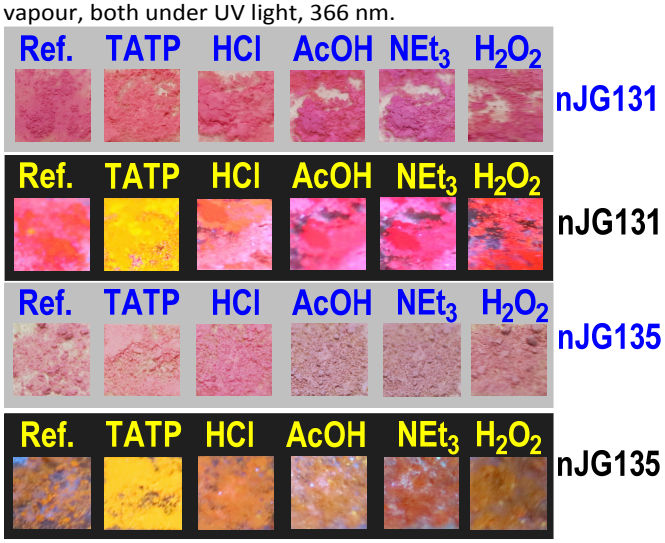

Figure 5 Detection of TATP in the gas phase by the colour and fluorescence changes of modified silica nanoparticles **nJG131/nJG135** with vapours of TATP, acids, amine and hydrogen peroxide. *First row*: **Ref.**: pristine **nJG131**; **TATP**: **nJG131** in the presence of the vapours of TATP; **HCl**: **nJG131** in the presence of the vapours of HCl 35% w/v; **AcOH**: **nJG131** in the presence of the vapours of glacial acetic acid; **NEt_3**: **nJG131** in the presence of the vapours of triethylamine; **H_2O_2**: **nJG131** in the presence of the vapours of H_2O_2, all under white light; *Second row:* same experimental conditions than in the first row, but under a UV lamp, 366 nm. *Third row*: **Ref.**: pristine **nJG135**; **TATP**: **nJG135** in the presence of the vapours of TATP; **HCl**: **nJG135** in the presence of the vapours of HCl 35% w/v; **AcOH**: **nJG135** in the presence of the vapours of glacial acetic acid; **NEt_3**: **nJG135** in the presence of the vapours of triethylamine; **H_2O_2**: **nJG135** in the presence of the vapours of H_2O_2, all under white light. *Fourth row*: same experimental conditions than in the third row, but under a UV lamp, 366 nm.

Except for a slight sensitivity to strong acid vapour, seen as a small increase in fluorescence emission, the most remarkable finding was a dramatic increase in the fluorescence emission of **nJG131** and **nJG135** in the presence of TATP vapour in a very selective fashion. Acetic acid, triethylamine or hydrogen peroxide vapours did not show noticeable fluorescence changes under the same conditions, even more, NEt_3 or AcOH reversed the action of HCl on the materials. Common solvents such as diethylether or acetone did not show any effect other than moistening of the silica by polar solvents with no change in fluorescence. Therefore, both materials were best suited for the detection of TATP vapour in a stream flow at one third of the maximum saturation equilibrium concentration of TATP (reported as 600 μgL^{-1}).[1a] Steady state spectra in Figure 6 showed a clear increase in the emission intensity in both cases, nJG131/nJG135 in the presence of TATP, very little increase of intensity in the presence of HCl and no change in the presence of H_2O_2. The quantitative increase in fluorescence with the solid materials was performed by measurement of quantum yield differences between samples, by repeating three times each sample until the error was lower to 2%. Consequently, for **nJG131** the overall increase of the quantum yield in the presence of TATP vapour was $\Phi_{nJG131+TATP}/\Phi_{nJG131}$ = 3.5; for **nJG135** the overall increase of the quantum yield in the presence of TATP vapour was $\Phi_{nJG135+TATP}/\Phi_{nJG131}$ = 3.1; for comparison, the overall increase of the quantum yield in the presence of HCl vapour was much lower, $\Phi_{nJG131+HCl}/\Phi_{nJG131}$ = $\Phi_{nJG135+HCl}/\Phi_{nJG131}$ = 1.6. In all cases, the increase in fluorescence in the presence of TATP vapour was sufficient for reliable measurements.

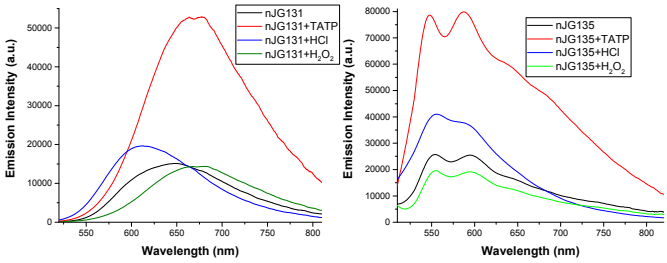

Figure 6 Response in fluorescence of **nJG131/nJG135** and TATP, HCl or H_2O_2. **nJG131**: λ_{exc} = 492 nm. **nJG135**: λ_{exc} = 495 nm.

Similarly, we tested colour and fluorescence qualitative and quantitative changes of solid plates **pJG131** and **pJG135** in the presence of TATP in the gas phase and compared them to the changes in the presence of HCl and H_2O_2 vapour. Albeit the shape of the particles moved from roughly 20 nm to 20 µm, the homogeneity of the plates could lead to an easier managing of the samples. The conditions were as in previous experiments, this time with 20 mm x 20 mm plates, the results are shown in Figure 7. We compared the results with the adsorbed colorants in plates, **aJG125** and **aPC63**, in the same conditions, also shown in Figure 7.

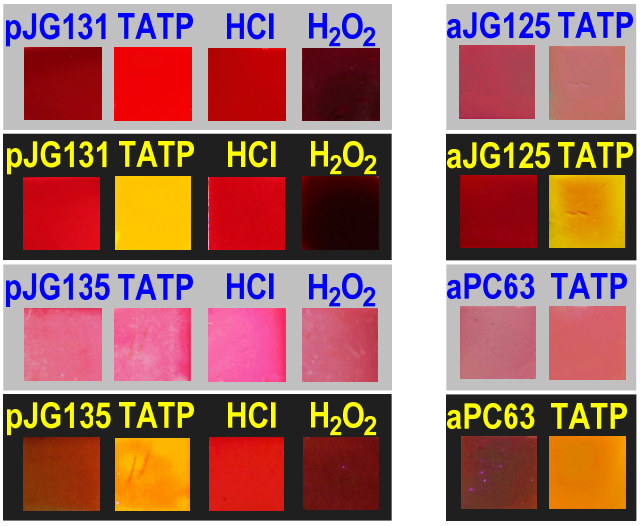

Figure 7 Detection of TATP in the gas phase by the colour and fluorescence changes of silica plates with vapours of TATP, HCl and hydrogen peroxide: *Left column*: **pJG131/pJG135**. *Right column*: **aJG125/aPC63**. *First row*: pristine **pJG131**; **TATP**: **pJG131** in the presence of the vapours of TATP; **HCl**: **pJG131** in the presence of the vapours of HCl 35%; **H_2O_2**: **pJG131** in the presence of the vapours of H_2O_2; pristine **aJG125**; **TATP**: **aJG125** in the presence of the vapours of TATP, all under white light; *Second row:* same experimental conditions than in the first row, but under a UV lamp, 366 nm. *Third row*: pristine **pJG135**; **TATP**: **pJG135** in the presence of the vapours of TATP; **HCl**: **pJG135** in the presence of the vapours of HCl 35%; **H_2O_2**: **pJG135** in the presence of the vapours of H_2O_2, pristine **aPC63**; **TATP**: **aPC63** in the presence of the vapours of TATP, all under white light. *Fourth row*: same experimental conditions than in the third row, but under a UV lamp, 366 nm.

Again the main features are a dramatic increase in the fluorescence emission of **pJG131** and **pJG135** in the presence of TATP vapour in a very selective fashion and a slight sensitivity to strong acid vapour, seen as a small increase in fluorescence emission. Acetic acid or triethylamine vapours did not show noticeable fluorescence changes (not shown). On the other hand, hydrogen peroxide vapour, under the same conditions, showed a remarkable decrease in the initial fluorescence of the materials. The adsorbed colorants **aJG125** and **aPC63** showed similar features, albeit the initial colours of plates were less pronounced. Therefore, both types of materials were suited for the detection of TATP vapour but the functionalized silica samples had better performance. Steady state spectra in Figure 8 showed the increase in the emission intensity of **pJG131/pJG135/aJG125/aPC63** in the presence of TATP or HCl. The quantitative increase in fluorescence with the solid materials was performed by measurement of quantum yield differences between samples, by repeating three times each sample until error was lower to 2%. Consequently, for **pJG131** the overall increase of the quantum yield in the presence of TATP vapour was $\Phi_{pJG131+TATP}/\Phi_{pJG131}$ = 3.4; for **pJG135** the overall increase of the quantum yield in the presence of TATP vapour was $\Phi_{pJG135+TATP}/\Phi_{pJG131}$ = 3.5; for comparison, the overall increase of the quantum yield in the presence of HCl vapour was much lower, $\Phi_{pJG131+HCl}/\Phi_{pJG131}$ = 1.0; $\Phi_{pJG135+HCl}/\Phi_{pJG131}$ = 1.6. The adsorbed colorants on silica gave similar results. In all cases, the increase in fluorescence in the presence of TATP vapour was sufficient for reliable measurements.

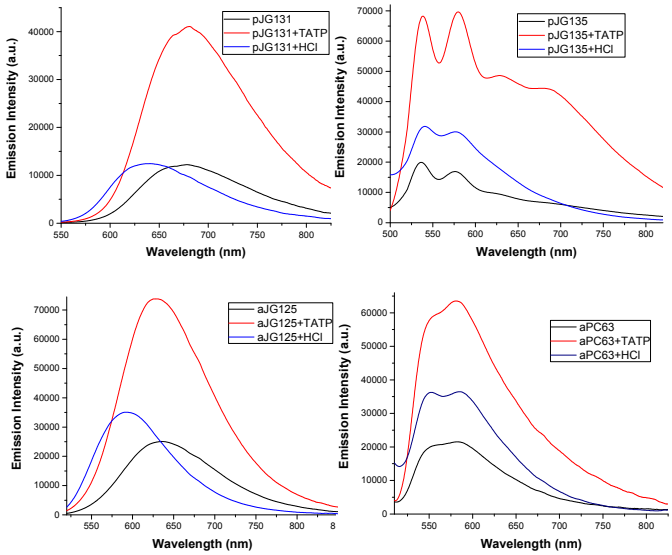

Figure 8 Response in fluorescence of **pJG131/pJG135** and TATP or HCl. **nJG131**: λ_{exc} = 438 nm. **nJG135**: λ_{exc} = 487 nm.

To understand the observed luminescent behaviour we performed quantitative fluorescence titration experiments in the solid/gas phase and in solution. In the solid/gas phase the experiment was performed to calculate the minimum amount of TATP that produced a detectable response between TATP gas and solid silica, measured in steady state. Fixed quantities of TATP where vaporized as in previous experiments in the presence of a sample containing 15 mg of **nJG131** silica nanoparticles in a single 100 mL flask under recirculating nitrogen (100 mL/min) for 10 minutes and the fluorescence increase of every silica sample was then measured (Figure 9).

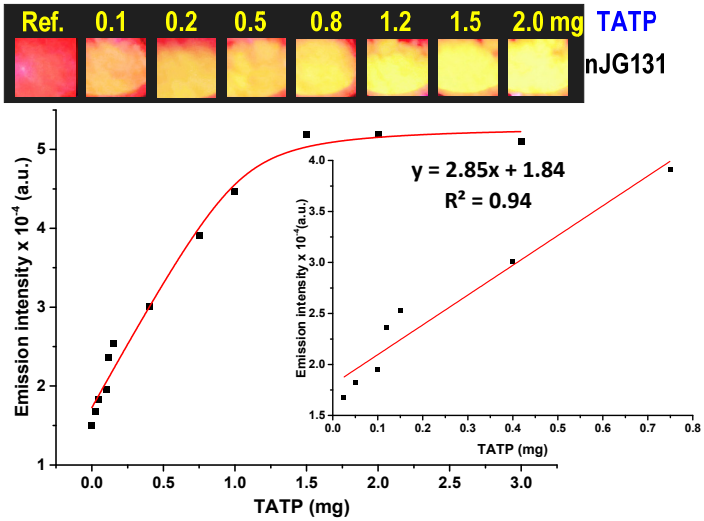

Figure 9 Upper: Qualitative effect of increasing amounts of TATP vapour on **nJG131** under a 366 nm UV light. Lower:

Fluorescent titration profile and calibration plot of **nJG131** with increasing amounts of TATP, λ_{exc} = 495 nm, λ_{em} = 620 nm.

By making a linear regression plot at low amounts of TATP the LOD was calculated by having a 5% or less of false positive/negative responses when detecting TATP. The calculations lead to a limit of detection of 0.12 mgL^{-1} (same method used in previous calculated LODs). Using less TATP amounts there was still signal but it gave very low repeatability because of the difficulty when handling low quantities of solid TATP. Therefore, 0.12 mgL^{-1} TATP in the experimental conditions represents a reliable minimum amount detected by the technique. In solution, we performed quantitative fluorescence titration experiments of **JG125** (2.5·µM solution in $CHCl_3$:MeOH 9:1, λ_{exc} = 500 nm) by adding increasing concentrations of TATP in the same solvent mixture (Figure 10) and compared the results to a similar titration with a common organic oxidant, *m*-chloroperbenzoic acid (MCPBA) (Figure 11).

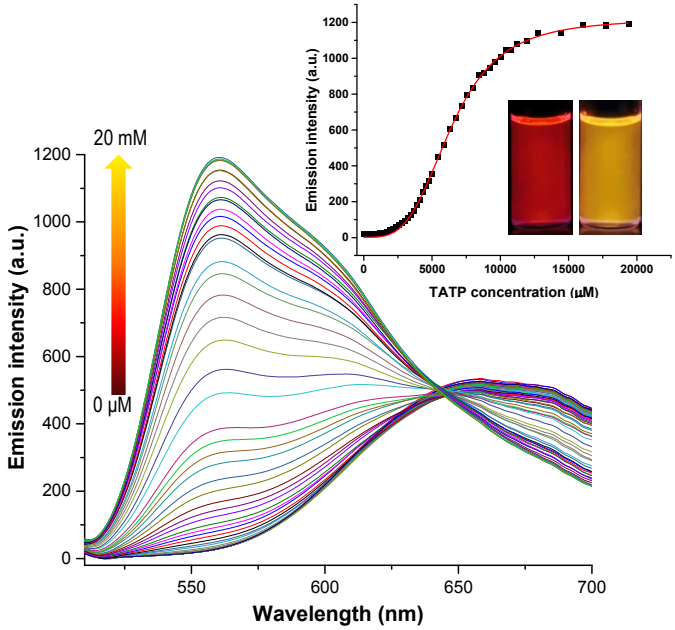

Figure 10 Fluorescent titration and titration profile at 556 nm of **JG125** (2.5 µM solution in $CHCl_3$:MeOH 9:1) under increasing concentrations of TATP. Inset pictures: Initial fluorescence of **JG125** (left) and after addition of 20 mM TATP (right).

TATP titration of a **JG125** solution showed the appearance of an emission in fluorescence at 556 nm and the decrease of the initial band at 665 nm after addition of excess TATP (Figure 9). The titration plot could be fitted to a sigmoidal curve with an asymptotic maximum after addition of a large excess of TATP (Figure 9). MCPBA titration of a **JG125** solution showed the appearance of an emission in fluorescence at 556 nm and the decrease of the initial band at 665 nm after addition of excess MCPBA (Figure 10). The titration plot could be fitted to an asymptotic curve by addition of excess of MCPBA (Figure 10).

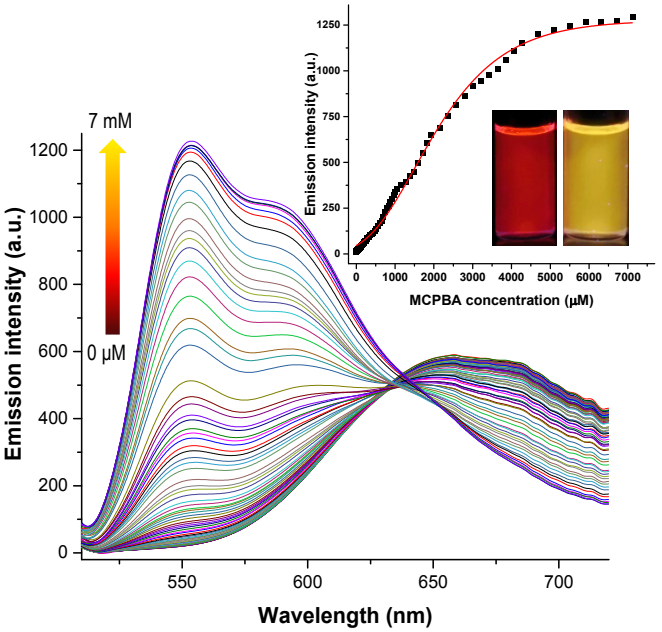

Figure 11 Fluorescent titration and titration profile at 556 nm of **JG125** (2.5 µM solution in $CHCl_3$:MeOH 9:1) under increasing concentrations of MCPBA. Inset pictures: Initial fluorescence of JG25 (left) and after addition of 20 mM MCPBA (right).

The main differences between both fluorescence titration corrected spectra were the presence of an isosbestic point for the TATP titration, which is not evident in the case of the MCPBA titration, and the steepest titration profile in the case of MCPBA acid (that afforded a limit of detection of 7.4 µM or 1.3 µg/mL) that reached the asymptotic maximum at a much lower concentration of oxidant. But generally speaking both titration curves were closely related, indicating in both cases an oxidation process of the fluorogenic probe **JG125** and in this case the higher oxidative ability of MCPBA with respect to TATP, as it is commonly accepted. The differences were even larger in the case of **PC63** (see the Supporting Information Figures S50-S51) supporting an oxidation of the dyes with an increase of the fluorescence as the dye is oxidized. In support for the oxidative nature of the detection mechanism we performed cyclic voltammetry experiments of **JG125**/**JG125d** as well as DFT calculations on the structure **JG125**/**JG125d** in its neutral state and the first oxidation state, and compared all results in search of an explanation of the luminescent behaviour of the dye in the presence of TATP. Cyclic voltammetry (See Supporting Information Figures S63-S64) showed important differences between **JG125** and **JG125d**. While **JG125** underwent a reversible oxidation at E° = +1.13 V, **JG125d** showed an irreversible oxidation wave with a value of E_{pk} = +1.01 V. This different behaviour was assigned to the presence or absence of the N-H bond. The radical cation formed by the one-electron oxidation of the secondary amine in **JG125d** should be very reactive leading to the observed electrochemical irreversibility and, therefore, the E_{pk} value could not relate directly to thermodynamic values. These values indicate an estimated difference between the oxidation potential of both compounds of 0.12 V. To know the position

of the oxidation process we performed quantum chemical calculations on structures **JG125** and **JG125d**. Optimization of compounds was carried out separately as neutral and radical cation in DFT calculations at the B3LYP[23]/6-31(d,p) level with simultaneous computation of PCM solvation[24] energies in dichloromethane, by using Gaussian 09, Revision D.01.[25] Each structure was verified to be a true minimum by the absence of imaginary frequencies in the vibrational analysis. Figure 12 displays the HOMO and the SOMO for **JG125**. Similar plots were calculated for **JG125d** (see Supporting Information Figures S66-S67). As expected, these two molecular orbitals display a similar topology and both orbitals are centered on the PDI core and the pyridine ring with important participation of the piperazine nitrogen atom bonded to the position 2 of the pyridine ring. There is, as well, a small participation of orbitals belonging to the oxygen atoms of the bisimide fragment.

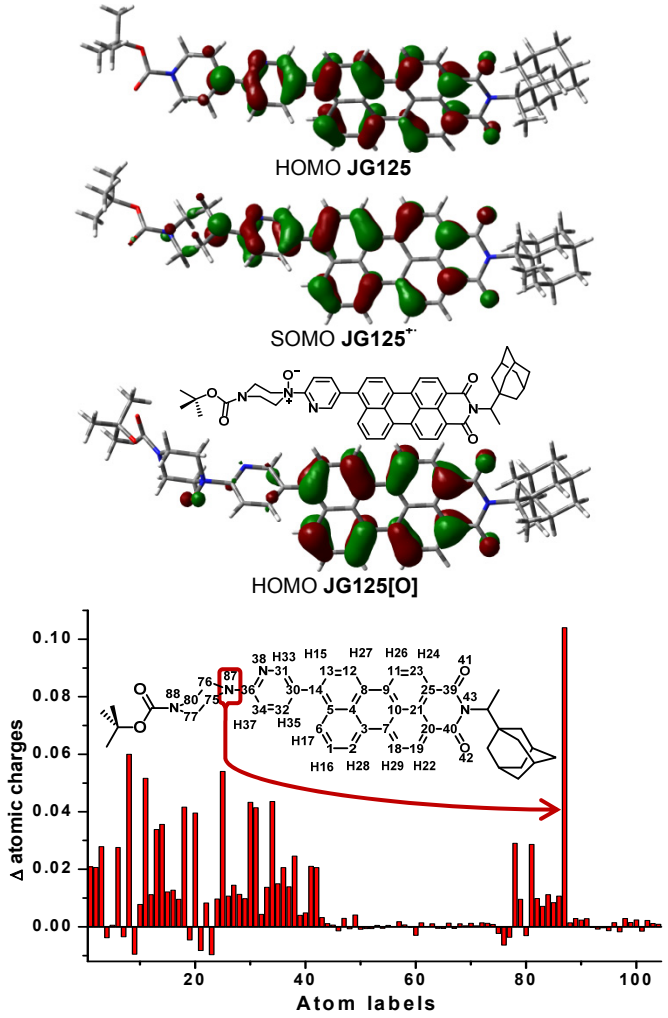

Figure 12 DFT calculated HOMO and SOMO plots for compound **JG125**/**JG125**$^{+\cdot}$ and HOMO plot of **JG125[O]**. NBO plot of differences between radical and neutral charges for every atom in **JG125**/**JG125**$^{+\cdot}$. Outer groups are not labelled.

The most important difference is the small participation of the orbitals of the N-H bond of the piperazine in the non-protected compound **JG125d** while the protection with Boc of the amine in **JG125** cancels this contribution to the HOMO. The difference in the structure of HOMOs between both compounds stabilizes the HOMO of **JG125** in 0.04 eV. The difference in the reversibility observed in the electrochemistry can be related to the observed differences in the HOMO of **JG125**/**JG125d** as well. The oxidation process affects the charge of the atoms with orbitals participating in the HOMO, displaying an increase of the positive electric charge of these atoms. The NBO[26] analysis showed the highest increase in the charge, after the removal of one electron, located on the piperazine nitrogen atom directly bonded to the position 2 of the pyridine ring (See N87 position in Figure 12). This atom showed an increase in its charge of 0.104 for **JG125** (its natural charge value changed from -0.458 in the neutral compound to -0.354 in the oxidized radical cation) and 0.124 in compound **JG125d** (variation from -0.454 in the neutral compound to -0.330 in the oxidized radical cation). It is expected that the oxidation by TATP will start on this nitrogen atom. To confirm the oxidation, we subjected a small sample of **JG125** to reaction with excess TATP and sent the residue to MALDI-TOF mass spectrometry, from which a peak at m/z 761.42, corresponding to the protonated N-oxide of **JG125**+O+H^{+}, was clearly seen (m/z calcd 761.37) (See Supporting Information, Figure S65). In order to understand the recovering of the luminescence observed after the reaction with TATP, the product of oxidation was modeled as a *N*-oxide on the N(87) (see Figure 12). The HOMO of **JG25[O]** was notably simplified as compared to the HOMO of **JG125** so the molecular orbital was centered on the perylenemonoimide fragment with a very small participation of the pyridine ring, displaying an electronic density distribution similar to a classic unsubstituted perylenemonoimide (Figure 12), confirming that the nitrogen oxidation stopped the charge transfer from its initial lone pair to the aromatic core of the PMI, interrupting the luminescence quenching already existing in **JG125** and therefore giving rise to the fluorescence increase experienced by **JG125** in the presence of TATP.

Conclusions

In conclusion, we have developed fluorogenic materials that were able to generate fluorescence in the presence of vapours of triacetone triperoxide, TATP, an improvised explosive used in terrorist attacks. The materials worked in a stream of vapours of TATP, giving a strongly fluorescent response. The fluorescent response given by the materials to the presence of TATP was permanent so it could be checked at any time after the TATP exposition. The mechanism consisted in the oxidation of an amino-substituted pyridine side group that quenched the fluorescence of the conjugated fluorophore by an intramolecular charge-transfer effect until it was oxidized with subsequent release of the original fluorescence of the perylenemonoimide/perylenediimide fluorophores. The materials are insensitive to hydrogen peroxide, the decomposition product of TATP, which is the common analyte used to detect TATP, but in itself it is not a threat. Therefore the reported materials detect TATP solely by the interaction

with the vapours of the intact explosive, minimizing the risk of a false positive detection.

Acknowledgements

We gratefully acknowledge financial support from the Ministerio de Economía y Competitividad, Spain (Project CTQ2015-71353-R) and Junta de Castilla y León, Consejería de Educación y Cultura y Fondo Social Europeo (Project BU051U16). J. G.-C. thanks Ministerio de Economía y Competitividad for his predoctoral FPU fellowship. This paper is dedicated to the memory of the late Dr. Stefano Marcaccini.

Notes and references

1 a) M. A. C. Härtel, T. M. Klapötke, B. Stiasny, J. Stierstorfer, *Propellants Explos. Pyrotech.* **2017**, *42*, 623–634; b) Homemade explosives, Indiana Intelligence Fusion Center, **2015**, 302 W. Washington St., Indianapolis, IN 46204, http://www.arkiaai.com/files/handouts/2016/Spring/home made_explosives.pdf, accessed 23rd August 2017.

2 F. Dubnikova, R. Kosloff, J. Almog, Y. Zeiri, R. Boese, H. Itzhaky, A. Alt, E. Keinan, *J. Am. Chem. Soc.* **2005**, *127*, 1146-1159.

3 a) K. Yeager, in: *Trace Chemical Sensing of Explosives*, (Ed.: R. L. Woodfin), Wiley, New Jersey, **2007**, Ch. 3, pp. 43-67; b) T.-H. Ong, T. Mendum, G. Geurtsen, J. Kelley, A. Ostrinskaya, R. Kunz, *Anal. Chem.* **2017**, *89*, 6482−6490; c) S. Sheykhi, L. Mosca, P. Anzenbacher Jr., *Chem. Commun.* **2017**, *53*, 5196–5199.

4 M. Ranstorp, M. Normark, Eds.: *Understanding Terrorism Innovation and Learning: Al-Qaeda and Beyond*, Routledge, Taylor & Francis Group LLC, 7625 Empire Drive, Florence, Kentucky 41042-2919, USA, **2015**, Chapt. 1, pp. 1-15.

5 a) R. Schulte-Ladbeck, M. Vogel, U. Karst, *Anal. Bioanal. Chem.* **2006**, *386*, 559–565; b) M. J. Kangas, R. M. Burks, J. Atwater, R. M. Lukowicz, P. Williams, A. E. Holmes, *Crit. Rev. Anal. Chem.* **2017**, *47*, 138–153; c) S. Girotti, E. Ferri, E. Maiolini, L. Bolelli, M. D'Elia, D. Coppe, F. S. Romolo, *Anal. Bioanal. Chem.* **2011**, *400*, 313–320; d) G. E. Collins, M. P. Malito, C. R. Tamanaha, M. H. Hammond, B. C. Giordano, A. L. Lubrano, C. R. Field, D. A. Rogers, R. A. Jeffries, R. J. Colton, S. L. Rose-Pehrsson, *Rev. Sci. Instrum.* **2017**, *88*, 034104(1-9).

6 M. Makinen, M. Nousiainen, M. Sillanpaa, *Mass Spectrom. Rev.* **2011**, *30*, 940-973.

7 D. Jiang, L. Peng, M. Wen, Q. Zhou, C. Chen, X. Wang, W. Chen, H. Li, *Anal. Chem.* **2016**, *88*, 4391−4399.

8 S. Tang, N. Vinerot, D. Fisher, V. Bulatov, Y. Yavetz-Chen, I. Schechter, *Talanta* **2016**, *155*, 235–244.

9 a) J. Tomlinson-Phillips, A. Wooten, J. Kozole, J. Deline, P. Beresford, J. Stairs, *Talanta* **2014**, *127*, 152–162; b) D. N. Correa, J. J. Melendez-Perez, J. J. Zacca, R. Borges, E. M. Schmidt, M. N. Eberlin, E. C. Meurer, *Propellants Explos. Pyrotech.* **2017**, *42*, 370–375; c) S. Hagenhoff, J. Franzke, H. Hayen, *Anal. Chem.* **2017**, *89*, 4210−4215.

10 A. Lichtenstein, E. Havivi, R. Shacham, E. Hahamy, R. Leibovich, A. Pevzner, V. Krivitsky, G. Davivi, I. Presman, R. Elnathan, Y. Engel, E. Flaxer, F. Patolsky, *Nature Commun.* **2014**, *5*, Art. No. 4195, doi:10.1038/ncomms5195.

11 a) H. Lin, K. S. Suslick, *J. Am. Chem. Soc.* **2010**, *132*, 15519–15521; b) Z. Li, W. P. Bassett, J. R. Askim, K. S. Suslick, *Chem. Commun.* **2015**, *51*, 15312–15315; c) J. R. Askim, Z. Li, M. K. LaGasse, J. M. Rankin, K. S. Suslick, *Chem. Sci.* **2016**, *7*, 199–206; d) V. Kumar, K.-H. Kim, P. Kumar, B.-H. Jeon, J.-C. Kim, *Coord. Chem. Rev.* **2017**, *342*, 80–105.

12 a) S, Parajuli and W. Miao, *Anal. Chem.* **2013**, *85*, 8008−8015; b) S. Malashikhin and N. S. Finney, *J. Am. Chem. Soc.* **2008**, *130*, 12846–12847.

13 a) A. Üzer, S. Durmazel, E. Ercag, R. Apak, *Sens. Actuators B* **2017**, *247*, 98–107; b) Z. Can, A. Uzer, K. Turkekul, E. Ercag, R. Apak, *Anal. Chem.* **2015**, *87*, 9589−9594; c) M. Xu, J.-M. Han, C. Wang, X. Yang, J. Pei, L. Zang, *ACS Appl. Mater. Interfaces* **2014**, *6*, 8708-8714.

14 a) E. Sella, D. Shabat, *Chem. Commun.* **2008**, 5701-5703; b) W. Xu, Y. Fu, Y. Gao, J. Yao, T. Fan, D. Zhu, Q. He, H. Cao, J. Cheng, *Chem. Commun.* **2015**, *51*, 10868-10870; c) J. Chen, W. Wu, A. J. McNeil, *Chem. Commun.* **2012**, *48*, 7310-7312; d) Y. Salinas, R. Martínez-Máñez, M. D. Marcos, F. Sancenón, A. M. Costero, M. Parra, S. Gil, *Chem. Soc. Rev.* **2012**, *41*, 1261-1296.

15 a) M. R. Rao, Y. Fang, S. De Feyter, D. F. Perepichka, *J. Am. Chem. Soc.* **2017**, *139*, 2421−2427; b) H. Q. Zhang, W. B. Euler, *Sens. Actuators B* **2016**, *225*, 553–562.

16 a) D. Lubczyk, C. Siering, J. Lörgen, Z. B. Shifrina, K. Müllen, S. R. Waldvogel, *Sens. Actuators B* **2010**, *143*, 561–566; b) D. Lubczyk, M. Grill, M. Baumgarten, S. R. Waldvogel, K. Müllen, *ChemPlusChem* **2012**, *77*, 102−105; c) B. A. G. Hammer, K. Müllen, *Chem. Rev.* **2016**, *116*, 2103−2140.

17 a) J. Wu, B. Kwon, W. Liu, E. V. Anslyn, P. Wang, J. S. Kim, *Chem. Rev.* **2015**, *115*, 7893−7943; b) Z. Yang, J. Cao, Y. He, J. H. Yang, T. Kim, X. Peng, J. S. Kim, *Chem. Soc. Rev.* **2014**, *43*, 4563−4601; c) Z. Köstereli, R. Scopelliti, K. Severin, *Chem. Sci.* **2014**, *5*, 2456–2460; d) F. Hof, *Chem. Commun.* **2016**, *52*, 10093−10108; e) D. Wu, A. C. Sedgwick, T. Gunnlaugsson, E. U. Akkaya, J. Yoon, T. D. James, *Chem. Soc. Rev.* **2017**, DOI: 10.1039/c7cs00240h.

18 a) S. Kaloyanova, Y. Zagranyarski, S. Ritz, M. Hanulová, K. Koynov, A. Vonderheit, K. Müllen, K. Peneva, *J. Am. Chem. Soc.* **2016**, *138*, 2881–2884; b) U. Lewandowska, W. Zajaczkowski, L. Chen, F. Bouillière, D. Wang, K. Koynov, W. Pisula, K. Müllen, H. Wennemers, *Angew. Chem. Int. Ed.* **2014**, *53*, 12537–12541; c) A. Bolag, N. Sakai, S. Matile, *Chem. Eur. J.* **2016**, *22*, 9006–9014; d) J. A. Hutchison, H. Uji-i, A. Deres, T. Vosch, S. Rocha, S. Müller, A. A. Bastian, J. Enderlein, H. Nourouzi, C. Li, A. Herrmann, K. Müllen, F. De Schryver, J. Hofkens, *Nature Nanotech.* **2014**, *9*, 131-136; e) U. Lewandowska, W. Zajaczkowski, W. Pisula, Y. Ma, C. Li, K. Müllen, H. Wennemers, *Chem. Eur. J.* **2016**, *22*, 3804–3809

19 a) K. Liu, Z. Xu, M. Yin, *Prog. Polym. Sci.* **2015**, *46*, 25-54; b) F. Würthner, C. R. Saha-Möller, B. Fimmel, S. Ogi, P. Leowanawat, D. Schmidt, *Chem. Rev.* **2016**, *116*, 962−1052; c) M. Sun, K. Müllen, M. Yin, *Chem. Soc. Rev.* **2016**, *45*, 1513−1528; d) F. Fernández-Lázaro, N. Zink-Lorre, A. Sastre-Santos, *J. Mater. Chem. A*, **2016**, *4*, 9336−9346; e) Y. Guo, Y. Li, O. Awartani, H. Han, J. Zhao, H. Ade, H. Yan, D. Zhao, *Adv. Mater.* **2017**, *29*, 1700309.

20 **PDIs:** a) S. Seifert, D. Schmidt, F. Würthner, *Chem. Sci.* **2015**, *6*, 1663-1667; b) D. Jänsch, C. Li, L. Chen, M. Wagner, K. Müllen, *Angew. Chem. Int. Ed.* **2015**, *54*, 2285–2289; c) L. You, D. Zha, E. V. Anslyn, *Chem. Rev.* **2015**, *115*, 7840–7892; d) W. Ma, L. Qin, Y. Gao, W. Zhang, Z. Xie, B. Yang, L. Liua, Y. Ma, *Chem. Commun.* **2016**, *52*, 13600–13603; **PMIs:** e) M. T. Vagnini, M. W. Mara, M. R. Harpham, J. Huang, M. L. Shelby, L. X. Chen, M. R. Wasielewski, *Chem. Sci.* **2013**, *4*, 3863–3873; f) Z. Liu, C. Tonnelé, G. Battagliarin, C. Li, R. A. Gropeanu, T. Weil, M. Surin, D. Beljonne, R. Lazzaroni, M. Debliquy, J.-M. Renoirt, K. Müllen, *J. Phys. Chem. B* **2014**, *118*, 309−314; g) A. Sanguineti, M. Sassi, R. Turrisi, R. Ruffo, G. Vaccaro, F. Meinardi, L. Beverina, *Chem. Commun.* **2013**, *49*, 1618–1620; h) P. Shao, N. Jia, S. Zhang, M. Bai, *Chem. Commun.* **2014**, *50*, 5648−5651.

21 N. Gomes, Trace Detection of TATP Vapors Using a Low-Mass Thermodynamic Sensor. *Open Access Master's Theses*, **2017**, 1067. http://digitalcommons.uri.edu/theses/1067.

22 a) B. Díaz de Greñu, D. Moreno, T. Torroba, A. Berg, J. Gunnars, T. Nilsson, R. Nyman, M. Persson, J. Pettersson, I. Eklind, P. Wästerby, *J. Am. Chem. Soc.* **2014**, *136*, 4125–4128; b) B. Díaz de Greñu, J. García-Calvo, J. Cuevas, G. García-Herbosa, B. García, N. Busto, S. Ibeas, T. Torroba, B. Torroba, A. Herrera, S. Pons, *Chem. Sci.* **2015**, *6*, 3757–3764; c) P. Calvo-Gredilla, J. García-Calvo, J. V. Cuevas, T. Torroba, J.-L. Pablos, F. C. García, J.-M. García, N. Zink-Lorre, E. Font-Sanchis, A. Sastre-Santos, F. Fernández-Lázaro, *Chem. Eur. J.* **2107**, *23*, 13973–13979; d) J. García-Calvo, S. Ibeas, E.-C. Antón-García, T. Torroba, G. González-Aguilar, W. Antunes, E. González-Lavado, M. L. Fanarraga, *ChemistryOpen* **2017**, *6*, 562−570.

23 a) A. D. Becke, *J. Chem. Phys.* **1993**, *98*, 5648–5652; b) C. T. Lee, W. T. Yang, R. G. Parr, *Phys. Rev. B* **1988**, *37*, 785–789.

24 A. Capobianco. A. Velardo. A. Peluso. *Comput. Theor. Chem.* **2015**, *1070*, 68–75.

25 M. J. Frisch, G. W. Trucks, H. B. Schlegel, G. E. Scuseria, M. A. Robb, J. R. Cheeseman, G. Scalmani, V. Barone, B. Mennucci, G. A. Petersson, H. Nakatsuji, M. Caricato, X. Li, H. P. Hratchian, A. F. Izmaylov, J. Bloino, G. Zheng, J. L. Sonnenberg, M. Hada, M. Ehara, K. Toyota, R. Fukuda, J. Hasegawa, M. Ishida, T. Nakajima, Y. Honda, O. Kitao, H. Nakai, T. Vreven, J. A. Montgomery, Jr., J. E. Peralta, F. Ogliaro, M. Bearpark, J. J. Heyd, E. Brothers, K. Raghavachari, A. Rendell, J. C. Burant, S. S. Iyengar, J. Tomasi, M. Cossi, N. Rega, J. M. Millam, M. Klene, J. E. Knox, J. B. Cross, V. Bakken, C. Adamo, J. Jaramillo, R. Gomperts, R. E. Stratmann, O. Yazyev, A. J. Austin, R. Cammi, C. Pomelli, J. W. Ochterski, R. L. Martin, K. Morokuma, V. G. Zakrzewski, G. A. Voth, P. Salvador, J. J. Dannenberg, S. Dapprich, A. D. Daniels, O. Farkas, J. B. Foresman, J. V. Ortiz, J. Cioslowski, D. J. Fox, *Gaussian 09*, Revision D.01, Gaussian, Inc. Wallingford CT, **2013**.

26 E. D. Glendening, A. E. Reed, J. E. Carpenter, F. Weinhold, *NBO Version 3.1*.